Evaluation of ionomer distribution on porous carbon aggregates in catalyst layers of polymer electrolyte fuel cells

Park, Kayoung

Gao, Ruijing

So, Magnus

Noh, Tae Hyoung

他

出版情報：Journal of Power Sources Advances. 15, pp.100096-, 2022-05. Elsevier
バージョン：

Journal of Power Sources Advances 15 (2022) 100096

Contents lists available at ScienceDirect

Journal of Power Sources Advances

journal homepage: www.sciencedirect.com/journal/journal-of-power-sources-advances

Evaluation of ionomer distribution on porous carbon aggregates in catalyst layers of polymer electrolyte fuel cells

Kayoung Park, Ruijing Gao, Magnus So, Tae Hyoung Noh, Naoki Kimura, Yoshifumi Tsuge, Gen Inoue *

Department of Chemical Engineering, Faculty of Engineering, Kyushu University, 744 Motooka, Nishi-ku, Fukuoka, 819-0395, Japan

ARTICLE INFO

Keywords:
Polymer electrolyte fuel cells
Catalyst layer
Porous carbon
Carbon aggregate structure
Ionomer distribution
Simulation

ABSTRACT

Understanding ionomer distribution properties that facilitate proton conduction and oxygen transfer to Pt particles in the cathode catalyst layer (CCL) of the polymer electrolyte fuel cell (PEFC) is essential for optimized design of CCL with high cell performance. In this study, the model structure of Ketjen black (KB) as porous carbon was numerically simulated. After validating the model, the relationship between the weight ratio of ionomer/carbon (I/C) and ionomer coverage was investigated. Moreover, relative proton conductivity of simulated KB was compared with the reference data of Vulcan XC-72 (VB) as non-porous carbon. Under the same I/C ratio conditions, ionomer coverage significantly differed depending on the carbon support. Moreover, under the same carbon volume ratio conditions, simulated KB exhibited lower relative proton conductivity than VB because simulated KB had the lower ionomer volume ratio than that of simulated VB. The relationship between ionomer content and ionomer properties differ depending on the carbon support. The results of our study can contribute to designing an optimal catalyst layer.

1. Introduction

As a potential power device, polymer electrolyte fuel cells (PEFCs) have the advantages of high efficiency, no CO_2 and NO_x emissions, fast operating system, low operating temperature, and possibility of miniaturization. The main application of PEFCs is in fuel cell systems in automobiles. Because the PEFCs operate at low temperatures, carbon-supported Pt is generally used to catalyze the reactions at the anode and cathode in the PEFCs. However, using Pt catalysts is expensive and limits the popularization of PEFCs [1]. In PEFCs, the oxygen reduction reaction (ORR) is dominant at the cathode. Thus, extensive studies on the development of catalysts containing low or no Pt for the cathode and optimization of the cathode catalyst layer (CCL) to enhance Pt utilization have been reported [2–6]. To optimize the CCL, protons, electrons, and oxygens should be quickly transferred through ionomer, carbon, and pores, respectively, to the Pt surface on carbon. Moreover, the design is needed to be able to optimize the transfer path of these materials in the CCL of PEFCs.

Studies have been conducted on the properties of ionomers, such as distribution, coverage, thickness, and others [7–13]. These properties can be pathways of proton and oxygen transfer to the Pt surface. In our previous studies, we demonstrated that the ionomer morphologies affected the proton conductivity and were a dominant factor in the gas diffusivity to reach the Pt surface [8]. Properties such as ionomer coverage and thickness were numerically evaluated by simulating the structure of Vulcan XC-72 (VB) as a non-porous carbon [14]. First, the structural properties of the simulated VB, such as particle size distribution, anisotropy, specific surface area per weight, and pore volume, were verified by comparing with the experimental data. Then, the relationship between the ionomer/carbon (I/C) weight ratio and ionomer coverage were examined using the VB structure. As a result, the correlation equation for ionomer coverage could be estimated through the comparison with the reference (experimental) data. Furthermore, the effect of ionomer volume on relative proton conductivity was investigated using a simulated catalyst layer structure. Knowledge of the ionomer properties could contribute to designing the optimal catalyst layer. However, this study is limited to the properties of ionomer coating for non-porous carbon.

In this study, we performed numerical simulations to evaluate ionomer properties after coating Ketjen black (KB), which has a highly porous structure. In the numerical simulations of KB, carbon density was set as an input parameter to differentiate it from non-porous carbon

* Corresponding author.
E-mail address: ginoue@chem-eng.kyushu-u.ac.jp (G. Inoue).

https://doi.org/10.1016/j.powera.2022.100096
Received 12 February 2022; Received in revised form 7 April 2022; Accepted 15 April 2022
Available online 26 April 2022

during the catalyst-ink coating process. The carbon density value of VB was obtained from the literature as 1.7 g/cm^3 [15], whereas that of KB was obtained experimentally. Then, the KB aggregate structure was simulated and validated by comparison with the reference data. Although Pt particles were not considered in this study, the effect of porous carbon structure on ionomer coverage and distribution can be evaluated. This can provide insights into different ionomer properties that depend on the structural properties of support materials and contribute to the design of an effective CCL that is appropriate for the support conditions.

2. Methods

2.1. Experimental section

The value of carbon density including pores is essential in simulating the KB structure; however, it has not been reported in the literature. The values of carbon density can be estimated by the values of Pt loading, porosity, and thickness of the CCL. Therefore, a CCL containing KB-supported Pt catalysts (TEC10E50E, TKK, Tokyo, Japan) was fabricated using the doctor-blade method to estimate the carbon density of KB. First, catalyst ink was prepared by mixing and dispersing Pt/C, water, 1-propanol, and ionomer (5 mass% Nafion, Sigma-Aldrich) using ultrasonic homogenizer for 40 min. The values of solid fraction and I/C were 6% and 0.4, respectively. The catalyst ink was coated onto a polytetrafluoroethylene sheet using a coater and dried. The width, height, thickness, Pt/C weight ratio, Pt loading, catalyst weight, and porosity of the CCLs were obtained.

The necessary parameters for estimating the values of carbon density are summarized in Table 1. The porosity was measured using a pycnometer (AccuPyc II 1340, Micromeritics). The value of carbon density was estimated to approximately 0.6 g/cm^3. To verify this value, we compared the amount of dibutylphthalate (DBP) absorbed per 100 g of carbon when DBP was added to KB. The amount of DBP absorbed was estimated to be 334 cc/100 g, which is close to the value reported in the literature (360 cc/100g) [16]. Thus, the KB carbon density of 0.6 g/cm^3 was used as an input parameter for the KB aggregate simulations.

2.2. Numerical simulations

2.2.1. Simulation of KB aggregates

The KB aggregates were reconstructed as a basic structural element using in-house developed numerical model of the structure [17–20]. The KB aggregates were reconstructed using the probability density distribution, which is a function of the distance between the particles, based on the attraction and repulsion between the particles. As input parameters, the primary particle size, number of particles, and types of carbon structure were set to 30 nm, 50 particles, and branch structure, respectively. The space resolution was 2 nm, and the structural properties of the KB aggregates were obtained after the simulations.

2.2.2. Simulation of an ionomer coating

For the ionomer coating simulation for KB, a non-uniform model was applied to account for the non-uniform adhesion of the actual ionomer [21–23]. The curvature of the ionomer interface to the void space is constant, and the ionomer adheres to the curvature when the ionomer concentration is higher than the critical concentration for adhesion. This curvature value was automatically determined by the amount of ionomer, which depends on the I/C weight ratio. Because the space resolution was 2 nm, the minimum pore size was set to 2 nm. The assumptions for the simulations were as follows. The effect of solvent on ionomer structure change and adsorption, and the effect of carbon surface functionalizers on chemisorption were ignored. The surface area of carbon was significantly larger than that of Pt; hence, the effect of Pt particles on ionomer adsorption was negligible. In addition, the carbon and ionomer were well mixed in the solvent to avoid independent migration of the ionomer. Using the ionomer coating simulations, ionomer coverage and thickness were calculated. Moreover, ionomer-coated KB was visualized using MATLAB program. Finally, the relative proton conductivity ($\sigma^R_{H^+}$) of ionomer-coated KB was calculated using the following equation:

$$\sigma^R_{H^+} = \frac{\sigma^{eff}_{H^+}}{\sigma^{bulk}_{H^+}} = \frac{\varphi_{ionomer}}{\tau_{ionomer}} \quad (1)$$

where $\sigma^{eff}_{H^+}$ is effective transport property in porous media, $\sigma^{bulk}_{H^+}$ is effective transport property in bulk, $\varphi_{ionomer}$ is the volume ratio of the ionomer, and $\tau_{ionomer}$ is the tortuosity of the ionomer. We used the random work method to calculate the tortuosity and the ionomer connection.

Table 1
Structural information of the fabricated CCLs.

Parameters	Measured values
Width	1.5 cm
Height	1.5 cm
Thickness	12.6 mm
Weight	1.27 mg
Pt/C weight ratio	46.5 wt%
Carbon weight ratio (Pt/C)	53.5 wt%
Pt loading	0.21 mg/cm^2
Porosity	0.62

3. Results and discussion

Fig. 1 compares the structural properties of KB obtained from simulation. KB aggreages is generally composed of strongly bound primary carbon particles. Fig. 1(a) shows the branch structure of the simulated KB aggregate. This aggregate structure was similar to that of actual KB observed through transmission electron microscopy (TEM) shown in Fig. 1(b). This means that the KB aggregate can be reconstructed using simulation. Fig. 1(c) showed the simulated KB aggregate size. The size of the simulated KB aggregate was approximately 325 nm, which is within the range (100–500 nm) of the actual KB aggregate size measured by TEM of Neffati et al. [24]. As shown in Fig. 1(d), the peak value for the specific surface area per weight of simulated KB was approximately 850 m^2/g, which is close to the experimental value. In addition, the pore volumes of micropores (<2 nm) and mesopores (>2 nm) of simulated KB were 0.21 cc/g and 1.22 cc/g, respectively (Fig. 1(e)). These reference values [25] obtained from gas adsorption measurements such as N_2 adsorption were similar within the error range to the experimental values. With the development of the gas adsorption measurement method, recently a wide range of micropore evaluation can be detected by density functional theory (DFT) method. Among the various DFT methods, the non-local density functional theory (NL-DFT) technology has been reported as the most accurate technique for determining pore size distribution when the pore size distribution was different. This technology can be applied from 0.4 nm to 62 nm [24,26]. As show in Fig. 1(e), the mesopores of the simulated KB also had a very large pore volume compared to that of VB which is obtained by simulation [14].

Simulated KB structural properties such as aggregate size, surface weight, and pore volume were similar to the actual KB's experimental values, so they were verified as a support material to evaluate the properties of ionomer coating. In addition, the properties of the ionomer coating were evaluated on the basis of the simulated KB structure.

Fig. 2 shows ionomer distribution on the simulated KB surface with different I/C ratios. It can be seen that the ionomer was non-uniformly attached, and the amount of attached ionomer decreased with decreasing I/C.

In the case of ionomer distribution of simulated VB [14], the coverage was 0.87 at I/C 0.32 which is higher than the coverage of I/C

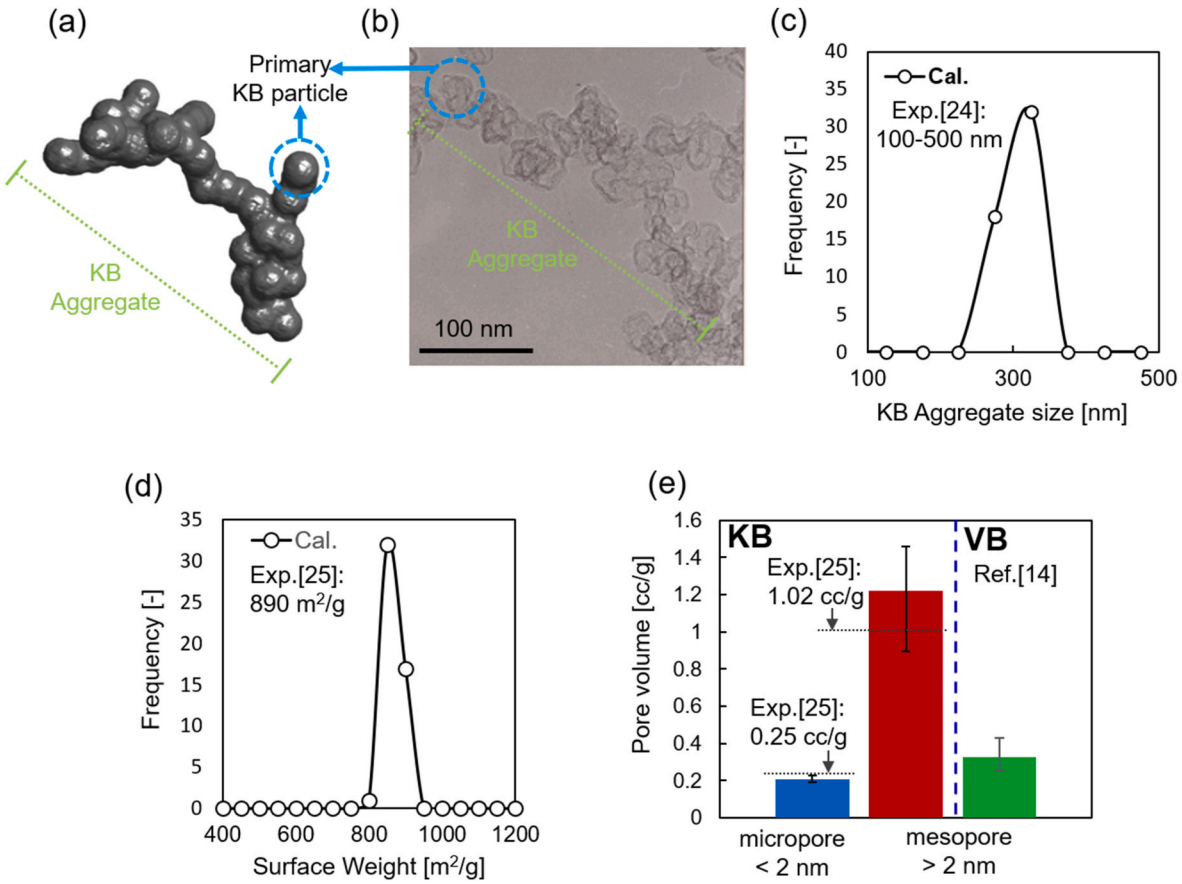

Fig. 1. Comparing the structural properties of simulated KB with those obtained from experiments. (a) Simulated KB structure, (b) TEM image of KB, (c) aggregate size distribution, (d) specific surface area per weight, and (e) pore volumes.

0.98 at KB. In other words, the ionomer coverage of VB and KB was significantly different.

Fig. 3 shows the changes in ionomer thickness and coverage with respect to the I/C ratio for simulated KB. The ionomer thickness and coverage of simulated VB with respect to the I/C ratio [14] are used as reference. The average thickness of the ionomer of KB was approximately 4 nm (Fig. 3(a)), while that of VB in the reference data was approximately 7 nm. The ionomer film of KB was approximately 1.8 times thinner than that of VB, which is consistent with the results of a previous study [27]. The reason for the thinner KB ionomer film than that of VB is the larger surface area of KB (approximately four times) than that of VB. Moreover, some ionomer could have been possibly absorbed into the nanopores of KB in the actual experiment. However, we did not consider the internal pores of KB in this study; thus, the possibility of ionomer absorption in nanopores was not examined.

Fig. 3(b) shows the comparison of the ionomer coverage of simulated KB at different I/C ratios with the reference data that was estimated through double-layer capacitance of catalyst [28]. The ionomer coverage values of the simulated KB were calculated for the I/C range of 0.2–1.0. This is because the ionomer volume ratio has a very low value below the I/C ratio of 0.2, resulting in no ionomer coverage due to space resolution of 2 nm. The ionomer coverage of the simulated KB decreased with decreasing I/C (particularly sharply below the I/C ratio of 0.4), and it is significantly off from the reference data value. In this simulation, it was assumed that all the ionomers covered the carbon support. It is reported that in the actual catalyst-ink coating process, ionomer does not coat all the carbon support; however, some ionomer is deposited and agglomerated. Harada et al. distinguished adsorbed ionomer from deposited ionomer using neutron scattering. The ratio of such ionomer was 50% each [9]; therefore, the ionomer content covering KB was converted to 50% and compared in Fig. 3(c). The ionomer covering of the simulated KB is in close agreement with the reference data at I/C = 0.42. Owing to the space resolution of 2 nm, ionomer coverage could not be seen at I/C less than 0.36. Thus, to predict the KB ionomer coverage at low I/C, the correlation between the I/C weight ratio and ionomer coverage was calculated as follows:

$$\theta_{ionomer} = 0.18\ln(R_{I/C}) + 0.74 (0.05 \le R_{I/C} \le 4.2) \quad (2)$$

Ionomer coverage does not exceed 1 and can be applied in the I/C range of 0.05–4.2. The ionomer coverage of the predicted lines of simulated KB using Equation (2) was in close agreement with the reference data at I/C = 0.05. At I/C = 1.0, the simulated and experimental values differed significantly; however, the experimental values of ionomer coverage for KB also exhibited differences depending on the measurement method. Thus, accurate estimation is difficult [25,29,30]. When KB and VB were compared, simulated KB exhibited lower ionomer coverage than that of the simulated VB under the same ionomer volume ratio conditions. This is due to the larger specific surface area per weight and lower carbon density of KB than those of VB. This indicates that the coverage property of ionomer depends on the types of carbon support with different I/C, and VB and KB cannot be compared on the same line. This result also shows that the amount of ionomer required for the optimization of the CCL varies with the types of carbon support.

Fig. 4 shows the relative proton conductivity of simulated KB and VB (reference values) [14] at different I/C ratios. The relative proton conductivity of both supports increases with increasing the carbon volume ratio. With the increase in the carbon volume ratio, the porosity decreased. The amount of ionomers coated increases and the distance between carbon aggregates also decreases with the increase in carbon volume ratio; thus, a proton conduction network is easily formed,

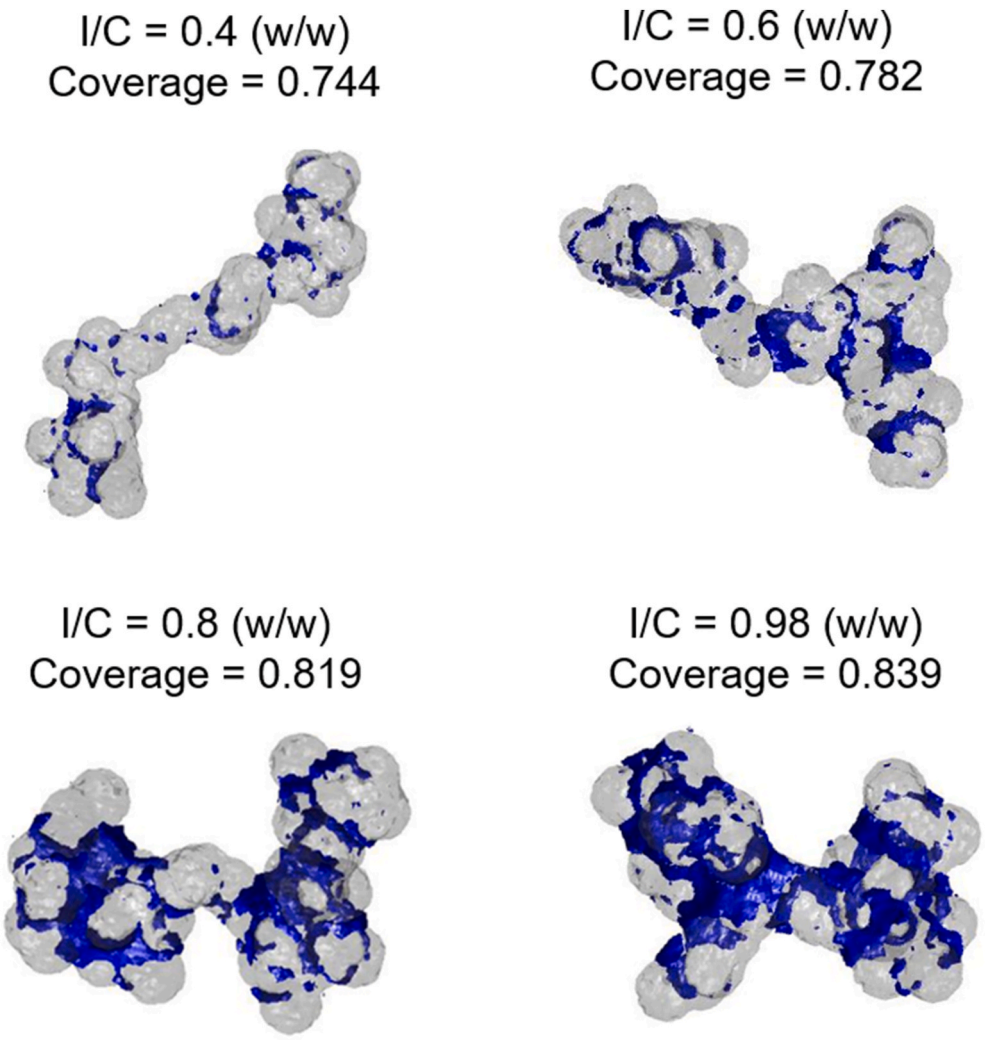

Fig. 2. Ionomer distribution on the surface of the simulated KB with different I/C ratio.

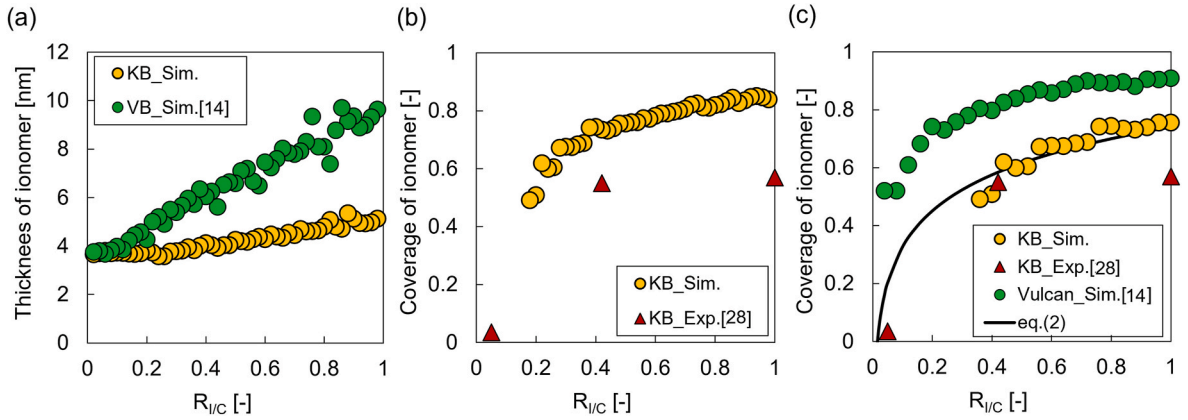

Fig. 3. Change of ionomer (a) thickness, (b) coverage of simulated KB with various I/C ratios. (c) conversion of Fig. 3(b) with various I/C ratios in the catalyst ink process. All data were compared with reference data.

resulting in an increase in proton conductivity.

In addition, it was found that there was a significant difference in relative proton conductivity between KB and VB. Under the same carbon volume ratio condition, the carbon density of KB (0.6 g/cm^3) showed lower than that of VB (1.7 g/cm^3), and thus the thickness of the catalyst layer of KB was higher than that of VB, which means an increase in the total volume of the CCL. This CCL's volume is used to calculate the ionomer volume ratio. The ionomer volume ratio is determined by the ratio of ionomer volume calculated from the I/C ratio, and CCL's volume. Because the KB and VB have the same ionomer volume, the KB with higher CCL's volume showed a lower ionomer volume ratio than that of VB. In other words, since KB had a lower ionomer volume ratio

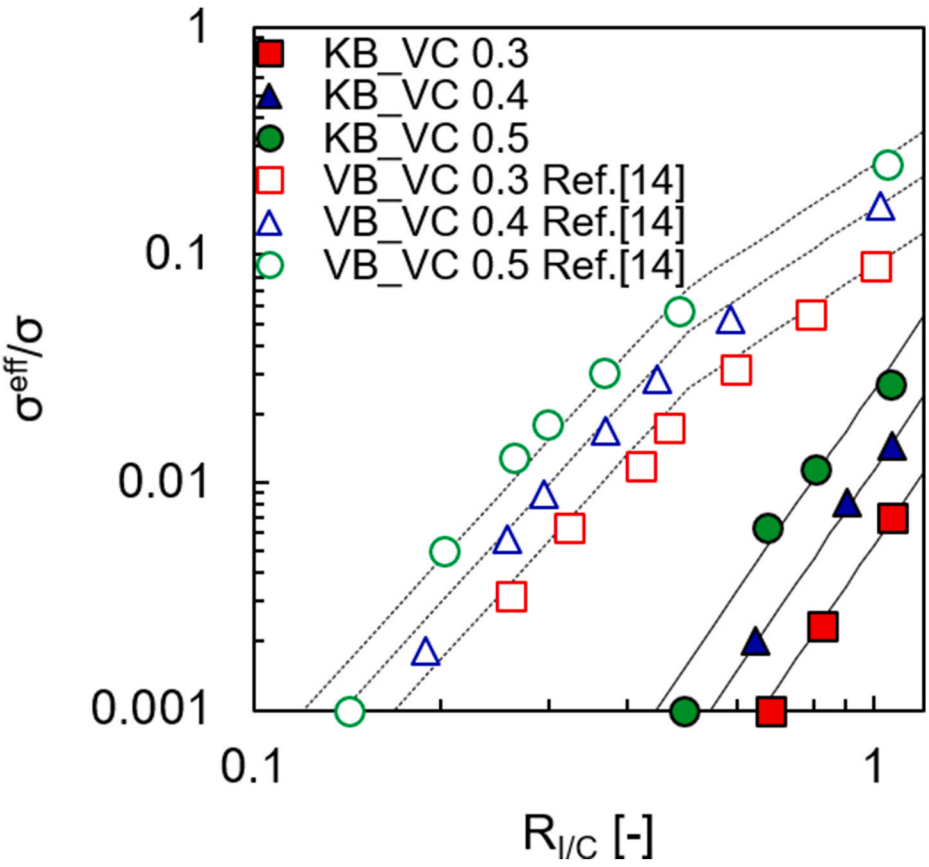

Fig. 4. Relationship between I/C ratios and relative proton conductivity in the CCLs with different carbon volume ratios of 0.3, 0.4, and 0.5.

than VB under the same carbon volume ratio condition, the relative proton conductivity of KB was significantly lower than that of VB. The effect of carbon support on proton conductivity has been investigated in experimental studies, and the results show that the proton conductivity of KB is lower than that of VB under the same I/C ratio conditions. This was due to the fact that the tortuosity of KB was higher than that of VB. Moreover, the ionomer adsorption inside the pores (4 nm) of KB did not affect the proton conductivity. Therefore, the amount of ionomer affecting the proton conductivity of KB was noticeably smaller than that of VB [31]. In this simulation, we did not consider the adhesion of the ionomer to the inner pore with pore sizes below 2 nm. However, it was confirmed that the ionomer volume ratio of KB was lower than that of VB under the same conditions, even if only the KB carbon density is considered. Considering these facts, the structural change of the carbon support by the carbon density and mesopore (>2 nm) affects the change of ionomer coverage and relative proton conductivity from the simulation technique. In our future work, we plan to perform detailed simulations of the ionomer considering the KB including nanopores.

4. Conclusions

The model structure of the porous material KB was numerically simulated, and the result of the simulations was compared with the experimental reference data to confirm the validity of the structure. The relationship between the I/C weight ratio and ionomer properties were investigated using KB, and the result was compared to the reference data of non-porous VB [14]. Owing to the large specific surface area of KB, the thickness and coverage of KB with different I/C ratios were found to be lower than those of VB, and the properties of ionomer varied with each carbon support. The relative proton conductivity was also examined using the simulated CCL structures at different I/C ratios. Under the same carbon volume ratio conditions, KB has a lower relative proton conductivity than that of VB. This is because the ionomer volume ratio of KB is lower than that of VB. Therefore, it is necessary to find the optimal amount of ionomer for each carbon support with different carbon density and mesopores to design an optimal catalyst layer.

Declaration of competing interest

The authors declare that they have no known competing financial interests or personal relationships that could have appeared to influence the work reported in this paper.

Acknowledgment

This research was supported by the New Energy and Industrial Technology Development Organization (NEDO), Japan (grant number P20003-20001327-0). This study collaborated to MEXT “Program for Promoting Researches on the Supercomputer Fugaku” (Fugaku Battery & Fuel Cell Project) (grant number JPMXP1020200301).

References

[1] M.K. Debe, Electrocatalyst approaches and challenges for automotive fuel cells, Nature 486 (2012) 43–51, https://doi.org/10.1038/nature11115.
[2] K. Park, H. Matsune, M. Kishida, S. Takenaka, Carbon-supported Pd-Ag catalysts with silica-coating layers as active and durable cathode catalysts for polymer electrolyte fuel cells, Int. J. Hydrogen Energy 42 (2017) 18951–18958, https://doi.org/10.1016/j.ijhydene.2017.06.046.
[3] E. Padgett, N. Andrejevic, Z. Liu, A. Kongkanand, W. Gu, K. Moriyama, Y. Jiang, S. Kumaraguru, T.E. Moylan, R. Kukreja, D.A. Muller, Editors’ choice—connecting fuel cell catalyst nanostructure and accessibility using quantitative cryo-STEM tomography, J. Electrochem. Soc. 165 (2018) F173–F180, https://doi.org/10.1149/2.0541803jes.
[4] S. Tzelepis, K.A. Kavadias, G.E. Marnellos, G. Xydis, A review study on proton exchange membrane fuel cell electrochemical performance focusing on anode and

cathode catalyst layer modelling at macroscopic level, Renew. Sustain. Energy Rev. 151 (2021) 111543, https://doi.org/10.1016/j.rser.2021.111543.
[5] S. Komini Babu, H.T. Chung, P. Zelenay, S. Litster, Resolving electrode morphology's impact on platinum group metal-free cathode performance using nano-CT of 3D hierarchical pore and ionomer distribution, ACS Appl. Mater. Interfaces 8 (2016) 32764–32777, https://doi.org/10.1021/acsami.6b08844.
[6] K. Park, Y. Wei, M. So, T.H. Noh, N. Kimura, Y. Tsuge, G. Inoue, Influence of surface structure on performance of inkjet printed cathode catalyst layers for polymer electrolyte fuel cells, J. Electrochem. Energy Convers. Storage. 19 (2022) 1–8, https://doi.org/10.1115/1.4052629.
[7] M. So, K. Park, Y. Tsuge, G. Inoue, A particle based ionomer attachment model for a fuel cell catalyst layer, J. Electrochem. Soc. 167 (2020), 013544, https://doi.org/10.1149/1945-7111/ab68d4.
[8] G. Inoue, M. Kawase, Effect of porous structure of catalyst layer on effective oxygen diffusion coefficient in polymer electrolyte fuel cell, J. Power Sources 327 (2016) 1–10, https://doi.org/10.1016/j.jpowsour.2016.07.037.
[9] M. Harada, S.I. Takata, H. Iwase, S. Kajiya, H. Kadoura, T. Kanaya, Distinguishing adsorbed and deposited ionomers in the catalyst layer of polymer electrolyte fuel cells using contrast-variation small-angle neutron scattering, ACS Omega 6 (2021) 15257–15263, https://doi.org/10.1021/acsomega.1c01535.
[10] H. Ren, Y. Teng, X. Meng, D. Fang, H. Huang, J. Geng, Z. Shao, Ionomer network of catalyst layers for proton exchange membrane fuel cell, J. Power Sources 506 (2021) 230186, https://doi.org/10.1016/j.jpowsour.2021.230186.
[11] D. Susac, V. Berejnov, A.P. Hitchcock, J. Stumper, STXM study of the ionomer distribution in the PEM fuel cell catalyst layers, ECS Meet. Abstr. MA2011–02 (2011), https://doi.org/10.1149/ma2011-02/16/823, 823–823.
[12] G. Doo, J.H. Lee, S. Yuk, S. Choi, D.H. Lee, D.W. Lee, H.G. Kim, S.H. Kwon, S. G. Lee, H.T. Kim, Tuning the ionomer distribution in the fuel cell catalyst layer with scaling the ionomer aggregate size in dispersion, ACS Appl. Mater. Interfaces 10 (2018) 17835–17841, https://doi.org/10.1021/acsami.8b01751.
[13] Z. Fang, M.S. Lee, J.Y. Kim, J.H. Kim, T.F. Fuller, The effect of carbon support surface functionalization on PEM fuel cell performance, durability, and ionomer coverage in the catalyst layer, J. Electrochem. Soc. 167 (2020), 064506, https://doi.org/10.1149/1945-7111/ab7ea3.
[14] G. Inoue, T. Ohnishi, M. So, K. Park, M. Ono, Y. Tsuge, Simulation of carbon black aggregate and evaluation of ionomer structure on carbon in catalyst layer of polymer electrolyte fuel cell, J. Power Sources 439 (2019) 227060, https://doi.org/10.1016/j.jpowsour.2019.227060.
[15] G. Heinrich, T.A. Vilgis, Contribution of entanglements to the mechanical properties of carbon black-filled polymer networks, Macromolecules 26 (1993) 1109–1119, https://doi.org/10.1021/ma00057a035.
[16] Y. Korai, Y.G. Wang, S.H. Yoon, S. Ishida, I. Mochida, Y. Nakagawa, Y. Matsumura, Effects of carbon black addition on preparation of meso-carbon microbeads, Carbon N. Y. 35 (1997) 875–884, https://doi.org/10.1016/S0008-6223(97)00036-5.
[17] G. Inoue, M. Kawase, Understanding formation mechanism of heterogeneous porous structure of catalyst layer in polymer electrolyte fuel cell, Int. J. Hydrogen Energy 41 (2016) 21352–21365, https://doi.org/10.1016/j.ijhydene.2016.08.029.
[18] M. So, K. Park, T. Ohnishi, M. Ono, Y. Tsuge, G. Inoue, A discrete particle packing model for the formation of a catalyst layer in polymer electrolyte fuel cells, Int. J. Hydrogen Energy 44 (2019) 32170–32183, https://doi.org/10.1016/j.ijhydene.2019.10.005.
[19] K. Park, M. So, M. Goto, S. Takenaka, Y. Tsuge, G. Inoue, Numerical analysis of silica coating effect on Pt cathode catalyst in polymer electrolyte fuel cells, J. Chem. Eng. Jpn. 54 (2021) 226–231, https://doi.org/10.1252/jcej.20we102.
[20] M. So, T. Ohnishi, K. Park, M. Ono, Y. Tsuge, G. Inoue, The effect of solvent and ionomer on agglomeration in fuel cell catalyst inks: simulation by the Discrete Element Method, Int. J. Hydrogen Energy (2019), https://doi.org/10.1016/j.ijhydene.2019.09.012.
[21] Y.C. Park, H. Tokiwa, K. Kakinuma, M. Watanabe, M. Uchida, Effects of carbon supports on Pt distribution, ionomer coverage and cathode performance for polymer electrolyte fuel cells, J. Power Sources 315 (2016) 179–191, https://doi.org/10.1016/j.jpowsour.2016.02.091.
[22] L. Guetaz, M. Lopez-Haro, S. Escribano, A. Morin, G. Gebel, D.A. Cullen, K.L. More, R.L. Borup, Catalyst-layer ionomer imaging of fuel cells, ECS Meet. Abstr. MA2015–02 (2015), https://doi.org/10.1149/ma2015-02/37/1471, 1471–1471.
[23] S. Takahashi, J. Shimanuki, T. Mashio, A. Ohma, H. Tohma, A. Ishihara, Y. Ito, Y. Nishino, A. Miyazawa, Observation of ionomer in catalyst ink of polymer electrolyte fuel cell using cryogenic transmission electron microscopy, Electrochim. Acta 224 (2017) 178–185, https://doi.org/10.1016/j.electacta.2016.12.068.
[24] R. Neffati, J.M.C. Brokken-Zijp, Structure and porosity of conductive carbon blacks, Mater. Chem. Phys. 260 (2021) 124177, https://doi.org/10.1016/j.matchemphys.2020.124177.
[25] T. Soboleva, X. Zhao, K. Malek, Z. Xie, T. Navessin, S. Holdcroft, On the micro-, meso-, and macroporous structures of polymer electrolyte membrane fuel cell catalyst layers, ACS Appl. Mater. Interfaces 2 (2010) 375–384, https://doi.org/10.1021/am900600y.
[26] Y.J. Heo, S.H. Yeon, S.J. Park, Defining contribution of micropore size to hydrogen physisorption behaviors: a new approach based on DFT pore volumes, Carbon N. Y. 143 (2019) 288–293, https://doi.org/10.1016/j.carbon.2018.11.019.
[27] F. Du, T.A. Dao, P.V.J. Peitl, A. Bauer, K. Preuss, A.M. Bonastre, J. Sharman, G. Spikes, M. Perchthaler, T.J. Schmidt, A. Orfanidi, Effects of PEMFC operational history under dry/wet conditions on additional voltage losses due to ionomer migration, J. Electrochem. Soc. 167 (2020) 144513, https://doi.org/10.1149/1945-7111/abc83f.
[28] T. Soboleva, K. Malek, Z. Xie, T. Navessin, S. Holdcroft, PEMFC catalyst layers: the role of micropores and mesopores on water sorption and fuel cell activity, ACS Appl. Mater. Interfaces 3 (2011) 1827–1837, https://doi.org/10.1021/am200590w.
[29] S. Ott, A. Bauer, F. Du, A. Dao, M. Klingenhof, Impact of carbon support mesoporosity on mass transport and performance of PEMFC cathode catalyst layers, 2021, pp. 4759–4769, https://doi.org/10.1002/cctc.202101162.
[30] M.A. Scibioh, I.H. Oh, T.H. Lim, S.A. Hong, H.Y. Ha, Investigation of various ionomer-coated carbon supports for direct methanol fuel cell applications, Appl. Catal. B Environ. 77 (2008) 373–385, https://doi.org/10.1016/j.apcatb.2007.08.010.
[31] Y. Liu, C. Ji, W. Gu, J. Jorne, H.A. Gasteiger, Effects of catalyst carbon support on proton conduction and cathode performance in PEM fuel cells, J. Electrochem. Soc. 158 (2011) B614–B621, https://doi.org/10.1149/1.3562945.